Binary blazed reflection gratings

M. Collischon, H. Haidner, P. Kipfer, A. Lang, J. T. Sheridan, J. Schwider, N. Streibl, and J. Lindolf

A reflection grating with a binary surface profile is presented that has high diffraction efficiency. The measured intensity for the +1st diffracted order was 77%. The binary grating is composed of a minilattice with feature sizes comparable with the wavelength of the incident light. The overall structure is designed in such a way that it imitates a conventional blazed grating. The grating also has interesting polarization properties. The main part of the TE-polarized light is diffracted into the 1st diffracted order, and most of the TM-polarized light remains in the 0th diffracted order. The measurements of the grating are compared with rigorous diffraction theory and found to be in reasonable agreement.

1. Introduction

Recently[1–3] the manufacture of dielectric gratings has been proposed in which each period is composed of a minilattice with a variable duty cycle and binary surface profile. Such elements have an advantage compared with conventional blazed gratings, which are known to show such high diffraction efficiency that only one microlithographic fabrication step is necessary to produce such gratings. The minilattice is based on a zero-order grating, and its behavior is similar to a dielectric material. By varying the duty cycle of the minilattice, the effective refractive index of the microstructure can be changed. In this way a binary grating can be made that behaves like an artificial dielectric material with a distributed index. In fact similar ideas have arisen previously in the area of micrometer waves.[4–6]

In this paper this idea is reapplied to create metallic binary blazed gratings as shown in Fig. 1 in principle. To understand the operation of these gratings, first we investigate the physics of the minilattices, which in this case are metallic zero-order gratings.

In Section 2 the theory of such binary blazed gratings is treated briefly. The subject of Section 3 is the fabrication method of such a grating. In Section 4 the results of measurements are compared with rigorous diffraction theory. The disagreements between theory and experiment are discussed, and some possible applications of the grating are presented.

2. Theory

The theory of these devices was developed in a previous publication.[7] Therefore in this section only a cursory version of the approximate model is presented so that it is possible to understand the grating operation.

In Fig. 1 a single period of such a binary blazed grating is shown. The height of the grating structure is h, and the overall grating period is d_1, which corresponds to a deflection angle $\sin(\varphi_1) = d_1/\lambda$ for the first order. The grating is composed of a minilattice with M binary (rectangular) grooves and a period d_2. Each of these grooves has a variable width $d_{3,m}$, where m is the index number of each individual microstructure; d_2 is assumed to be less than the wavelength of the incident light, so that all nonzero diffraction orders of the microstructure are evanescent. The refractive index above the grating is assumed to be $n_1 = 1$. The grating is designed to imitate a highly efficient blazed grating. To understand the operation of such a complicated structure, one must first understand the operation of metallic zero order gratings (Fig. 2), i.e., a minilattice with constant groove width d_3. If a plane wave is normally incident on such a grating, besides absorption, all the energy of the input beam is reflected into the zeroth diffraction order. The duty cycle t of this

The authors are with the Universität Erlangen-Nürnberg, D-91058 Erlangen, Germany. J. Lindolf is with the Institut für Technische Physik, Erwin-Rommelstrasse 2; the other authors are with the Physikalisches Institut, Staudtstrasse 7.

Received 28 December 1992; revised manuscript received 5 October 1993.

0003-6935/94/163572-06$06.00/0.

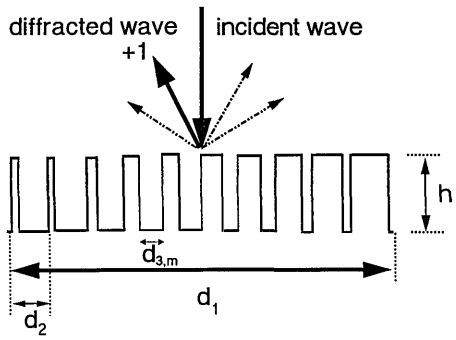

Fig. 1. Single period of a metallic binary blazed grating of height h with a superlattice period d_1 and a minilattice period d_2. The groove width of the mth microstructure is $d_{3,m}$.

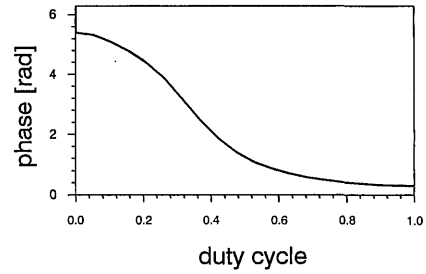

Fig. 3. Phase of the reflected zeroth order as a function of the duty cycle t. The grating period is $d_2 = 9$ μm and the height is $h = 5.3$ μm. The refractive index of the grating is $n = 0.22 + i6.7$ and the wavelength is $\lambda = 10.6$ μm. The wave is TE polarized and normally incident.

grating is defined as

$$t = (d_2 - d_3)/d_2, \tag{1}$$

which is the ratio of the filled metallic part of the microstructure to one period. The basic idea of this paper is the following: The phase of the reflected wave depends on the duty cycle of the minilattice period, and therefore by varying the duty cycle of the minilattice, one can fabricate a macroscopic blazed grating or more generally a kinoform. For a grating of period $d_2 = 9$ μm, $\lambda = 10.6$ μm, $n_1 = 1$, and $n_2 = 0.22 + i6.71$, the phase of the reflected zeroth order is calculated with the help of the differential method[8] as a function of the duty cycle t of the grating. $N = 11$ diffracted orders were included in the calculation to ensure convergence. The phase function relative to the duty cycle is shown in Fig. 3. The derivation of this phase function and approximations of this function were discussed in Ref. 7. Inverting the function numerically one can obtain the duty cycle as a function of the phase. For a blazed grating with period d_1 (Fig. 1) the phase of the reflected light of the superlattice should increase linearly from 0 to 2π within one period. Therefore we put for the phase of the mth microstructure

$$\varphi_m = 2\pi(m - 0.5)/M. \tag{2}$$

With the help of the inverted function and the phase values defined by Eq. (2) all M duty cycles for the M microstructures are calculated. Using this design process, Haidner *et al.*[7] showed that such a binary blazed grating can potentially have a high diffraction efficiency. But this design process may not be practical, because it does not take into account the existence of a minimum feature size, which arises from the available fabrication technology. Therefore slightly different duty cycles t_m optimized for a given fabrication technology should be used.

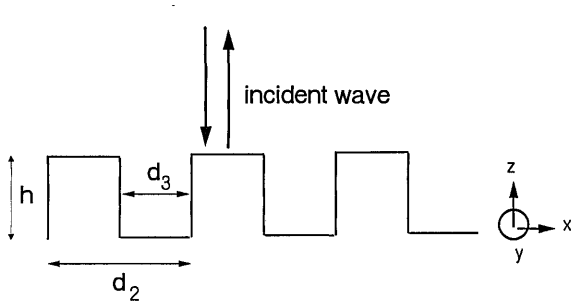

Fig. 2. Metallic zero-order grating. The height is h, and the period is d_2. The groove width is $d_3 < \lambda$.

3. Manufacturing the Grating

For the fabrication of the grating a minimum feature size of 1 μm was assumed, which is limited by the laser-pattern generator[9] available to us. For fabrication a fused-silica mask blank, with a 0.1-μm-thick chromium layer, was coated with a 0.5-μm-thick layer of photoresist and was exposed with the laser-pattern generator (LPG-15P from Micronics[9]) with a He–Cd laser. After resist development and chromium etching the fused silica was dry etched with reactive ion-etching equipment, PLASMA-LAB from Plasma Technology, with a CHF_3 process at 25-mTorr pressure and 195-W high-frequency power. Because of insufficient etch selectivity between the SiO_2 substrate and the photoresist layer, the maximum grating depth achievable was found to be ~2 μm.

For the desired gratings, depths of ~5 μm are required, and therefore the depth was increased by a self-alignment technique.[10] Using this technique, one coats the grating again with photoresist and exposes it from the back side. Developing and reactive ion etching are repeated until the desired depth is reached.

The last step in the process is cleaning the grating by removing the chromium followed by metallic coating (aluminum) by evaporation under several oblique angles, so that the perpendicular walls of the grating are also well coated with metal. Unfortunately the layer thickness achievable by this technique was not completely sufficient, which was observed by electrical conductivity measurements. The conductivity parallel and perpendicular to the grating lines shows a ratio of 50:1, which indicates a very thin coating on the perpendicular walls. Therefore some penetration of the incident light into the substrate might

Table 1. Shape of the Minilattices of the Grating[a]

Mini-lattice	Manufactured Grating Left (μm)	Manufactured Grating Right (μm)	Manufactured Grating Duty Cycle t_m	Calculated Grating Left (μm)	Calculated Grating Right (μm)	Calculated Grating Duty Cycle t_m
1	0	0.0	0.00	0	0.0	0.00
2	9	9.7	0.08	9	10.0	0.11
3	18	18.7	0.08	18	19.0	0.11
4	27	27.7	0.14	27	28.5	0.16
5	36	37.8	0.20	36	38.0	0.22
6	45	47.8	0.31	45	48.0	0.33
7	54	57.3	0.37	54	57.5	0.38
8	63	66.8	0.42	63	67.0	0.44
9	72	76.3	0.48	72	76.5	0.49
10	81	85.8	0.53	81	86.5	0.55

[a]Columns 2–4 refer to the experimentally realized component, and columns 5–7 describe the design. Apparently during the microlithographic fabrication some underetching systematically reduced all duty cycles.

occur, which results in light absorption and transmission into the substrate and therefore in a loss of diffraction efficiency.

The achieved depth of the grating was ~5.3 μm with an accuracy of 0.3 μm and was measured with an accuracy of 0.3 μm with a Linnik microscope. The grating period was 90 μm. The number of minilattices was $M = 10$. In Table 1 the parameters of the grating are given. The feature sizes were estimated by a scanning electron microscope. Because of underetching feature sizes appear that are less than the rated minimum feature of 1 μm. The first column denotes the particular mth microstructure being discussed. Columns 2, 3, and 4 are for the manufactured grating. Columns 5, 6, and 7 are for the proposed calculated grating with a 1-μm feature size.[7] In column 2 left indicates the left starting point of a feature, and in column 3 right indicates the right end point of a feature. Column 4 lists the duty cycle in each minilattice. In Fig. 4 a scanning electron micrograph of the manufactured grating is shown.

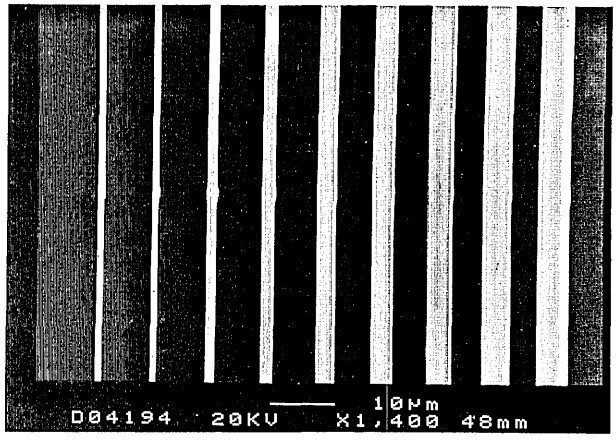

Fig. 4. Scanning electron micrograph of the manufactured grating.

4. Measurements and Comparison with Theory

The diffraction efficiencies of the gratings were measured with a CO_2 laser at a 10.6-μm wavelength. The incident intensity of the CO_2 laser was ~4 W/cm^2. To obtain polarized light, a conventional Brewster arrangement was used.

The refractive index of aluminum at $\lambda = 10.6$ μm is $n = 26.6 + i96.6$,[11] which is the refractive index of a nearly perfect conductor. For a comparison of the measurements two different rigorous diffraction theories were used:

(a) The differential method[8]: Because of the numerical problems in our implementation of the differential method it was not possible to use the refractive index above. Instead the arbitrary index $n = 0.22 + i6.7$ was used, which is also the refractive index of a good metal. For the calculations 61 diffracted orders were included.

(b) The modal method[12–14]: The grating was assumed to be perfectly conducting. The electric/magnetic field inside the rectangular grooves can be expressed with modes. In the calculations four modes were included in every groove. In the calculation 61 diffracted orders were taken into account.

In Fig. 5 diffraction efficiencies of the +1st, +10th, −9th, −10th diffraction order are shown as a function of the angle of incidence. The solid (dotted) curves are calculated with the differential method (modal method). Besides some differences for the −9th and −10th diffraction orders at high angles of incidence the agreement is good. The maximum of the diffraction efficiency of the +1st order is 84% for the differential method and 88% for the modal method.

The metallic coating of the considered grating is not as good a conductor as a perfect metal but a better conductor than the grating calculated with the differential method. Therefore we assume that the diffraction efficiencies can be calculated by both methods. The errors from the incorrect index are relatively small.

In Fig. 6 the diffraction efficiencies for normal incidence and TE-polarized light are shown (a) with a linear and (b) with a logarithmic scale. These theoretical estimations were produced with the differen-

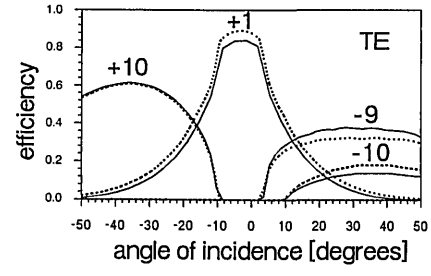

Fig. 5. Diffraction efficiencies of the +10th, +1st, −9th, and −10th diffraction orders as a function of the angle of incidence (classical diffraction). The solid (dotted) curves are calculated by the differential method (modal method).

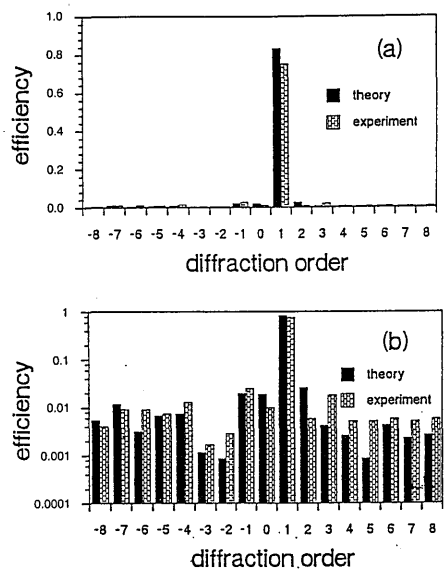

Fig. 6. Measured and calculated diffraction efficiencies for normal incidence and TE polarization. The grating period is $d_1 = 90$ μm, the wavelength is $\lambda = 10.6$ μm, and the height is $h = 5.3$ μm. The period of the $M = 10$ minilattice is $d_2 = 9$ μm. The minilattice parameters are described in detail in Table 1. The efficiencies are shown (a) with linear and (b) with logarithmic scaling.

tial method; $N = 61$ diffracted orders were included in the calculation to ensure convergence. The predicted theoretical diffraction efficiency of the +1st diffracted order is ~84% for a grating with the feature sizes given in Table 1. The experimentally measured diffraction efficiency at normal incidence for this diffraction order was ~75%. The measured value of the next strongest beam, the −1st order, is ~2.5% compared with 2% from the theory. The next strongest diffraction order is the +3rd order and shows ~1.8% measured efficiency compared with 0.7% from the theory. Summing up all measured diffraction efficiencies, we find only 87% of the input light. As stated, this appears to be mainly a result of the insufficient thickness of the metallic coating of the SiO_2 grating, which results in losses of the incident power in the grating. The nonlinearity of the detector may also have caused some errors. Unfortunately the detector available to us does not respond well to low light levels, since it is based on heating effects. Therefore the accuracy of the measurements of the diffraction orders with lower diffraction efficiency is reduced. Another reason for the discrepancy may be surface roughness, which leads to diffuse stray light. All these effects together result in a lower efficiency than predicted by theory. But it has also been stated that an incorrect refractive index was used in our numerical calculations, and the feature sizes, which were used for the numerical calculations, were measured with only limited accuracy. However, this use alone does not explain the apparent loss of 13% of the incident light.

In Fig. 7 the measured diffraction efficiency as a function of the polarization angle ω of the E field of

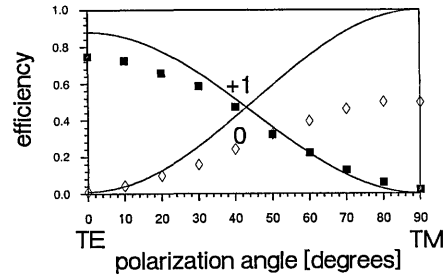

Fig. 7. Diffraction efficiency of the +1st diffracted order for normal incidence for the grating in Fig. 4. But now the polarization angle ω is changed from 0 (TE polarization) to 90 deg (TM polarization).

the incident beam relative to the grating vector **K** is presented. The calculated diffraction efficiencies of the +1st diffracted order are 88% (TE polarization) and 0% (TM polarization). The diffraction efficiencies of the 0th order are 1% (TE polarization) and nearly 100% (TM polarization). These diffraction efficiencies were calculated by the modal method. It is expected that the diffraction efficiency η depends sinusoidally on the polarization angle ω (Ref. 15):

$$\eta(\omega) = \eta_{TE} \cos^2(\omega) + \eta_{TM} \sin^2(\omega), \qquad (3)$$

where η_{TE} (η_{TM}) indicates the efficiency of a particular diffraction order at normal incidence for TE (TM) polarization. The curves belong to the theoretical predictions. The great differences between theoretical and measured values are striking.

The measured efficiency η_{TM} of the +1st order is ~2%, whereas η_{TM} of the 0th order is ~50%. (The theoretical prediction is nearly 100%.) From Fig. 7 we can see that the grating can be used as a polarizer, which diffracts most of the light for TM polarization into the 0th diffracted order and most of the light for TE polarization into the +1st diffracted order. When the polarization angle ω is changed, variable amounts of energy can be put in the 0th and +1st diffracted orders.

Now a set of measurements is described where the angle of incidence is varied (Fig. 8). Variation of the angle of incidence in the *xOz* plane is called classical diffraction, and variation of the angle of incidence in the *zOy* plane is called conical diffraction.

At first the case of classical diffraction is considered. The diffraction efficiencies as a function of the angle of incidence are examined. As has been said the grating period $d_1 = 90$ μm and the number of minilattices $M = 10$. The incident wavelength $\lambda = 10.6$ μm. The variation of the incident beam is in the *xOz* plane. In Fig. 8 the diffraction efficiencies of the +9th, +1st, 0th, −9th, and −10th diffraction orders are shown as functions of the angle of incidence. Measurements are compared with theoretical predictions calculated by the differential method. Under normal incidence 17 diffracted orders propagate. This fact can be calculated with the help of the

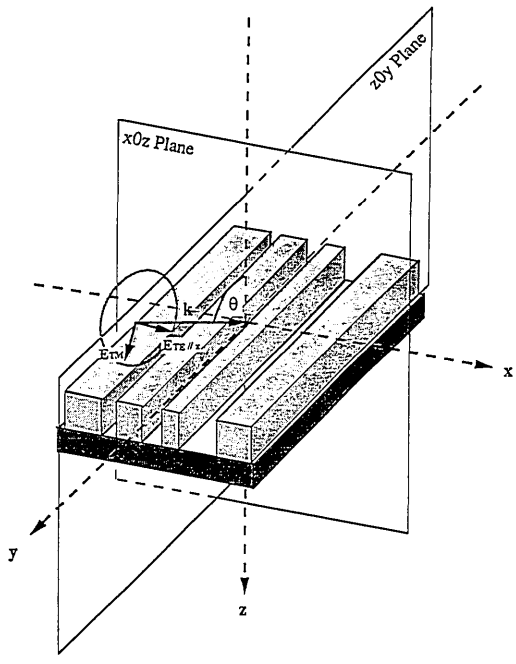

Fig. 8. Difference between classical (*xOz*-plane) and conical (*zOy*-plane) variation of the angle of incidence.

grating equation:

$$(2\pi/\lambda)\sin(\varphi_L) = (2\pi/\lambda)\sin(\varphi) + (2\pi/d_1)L, \quad (4)$$

where φ is the angle of incidence and φ_L is the angle of the Lth diffracted order. At normal incidence, $\varphi = 0$, the +10th, +9th, −9th, and −10th diffraction orders are evanescent. The ±9th diffracted order appears when $|\varphi| = 3.45$ deg, and the ±10th diffracted order occurs at ±10.25 deg. Now we return to the idea of the minilattices discussed in Section 2. The ±1st diffraction order of the minilattice appears when $|\varphi| = 10.25$ deg. The ±10th diffracted order of the superlattice and the ±1st diffraction order of the minilattice have the same diffraction angle and so correspond to each other. The duty cycle of the minilattice does not vary rapidly, and the diffraction spectrum roughly follows the spectrum for a perfectly periodic array. Therefore the strong increase of the ±10th diffracted orders can be explained by the fact that diffraction at the minilattice level occurs. The strong −9th diffracted order can be explained by the scatter of the strong +1st diffracted order by the minilattice.

By choosing a suitable minilattice period d_2, we can make the diffraction efficiency variation of the +1st diffracted order broader or narrower. As can be seen from Fig. 7 this function is almost flat until the strong diffracted orders start to propagate. At these angles the diffraction efficiency of the +1st diffracted order decreases very rapidly. Increasing the microstructure period d_2 decreases the width of the +1st diffracted order, and decreasing the size d_2 results in increasing the width of the function. Thus by changing the size d_2 we can design the angular selectivity of the +1st diffracted order. The diffraction efficiencies measured are always, especially for the +1st diffracted order, less than the theoretical predictions, probably because of losses in the grating. At an angle of ~2 deg the diffraction efficiency of the +1st diffracted order reaches 77%.

In Fig. 10 the diffraction efficiencies are shown as functions of the angle of incidence, but now for TM polarization. The variation of the incident beam is again in the *xOz* plane. The 0th diffracted order is the dominant order. The +1st diffracted order has almost vanished.

Now we describe a measurement in which the angle of the incident beam is varied in the *zOy* plane as shown in Fig. 8, which is the special case of conical diffraction.[16] For the conical angle of incidence of 0 deg the case corresponds to the case of classical diffraction in the *xOz* plane. As the conical angle of incidence is varied in the *zOy* plane, the E-field vector $\mathbf{E}_{TE}$ is always parallel to the x axis and the $\mathbf{E}_{TM}$ vector is always in the *zOy* plane. The $\mathbf{E}_{TE}$ and $\mathbf{E}_{TM}$ vectors are perpendicular to each other and to the $\mathbf{k}$ vector, and they define a plane shown as a disk in Fig. 6. An approximate model exists for the general case of conical diffraction by a perfect lossless metal and is described in Ref. 16.

For the particular case examined here this model predicts that the diffraction efficiencies of all diffracted orders should vary as if the input light was normally incident but had a wavelength of $\lambda/\cos(\Theta)$. This approximate model has been used for the calcula-

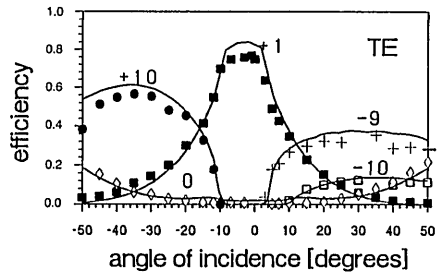

Fig. 9. Diffraction efficiencies as functions of the angle of incidence (*xOz* plane) for TE polarization (classical diffraction). The symbols are measured values; the curves are calculated by the differential method.

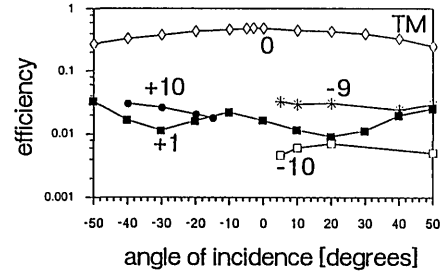

Fig. 10. Diffraction efficiencies for TM polarization as a function of the angle of incidence (*xOz* plane, conical diffraction). The symbols are measured values. A logarithmic scale is used.

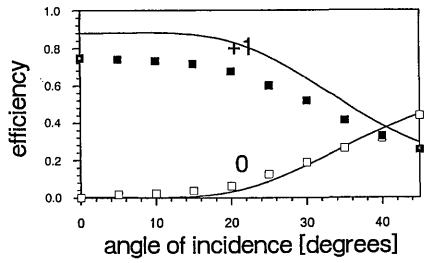

Fig. 11. Diffraction efficiencies as functions of the angle of incidence. The variation of the angle of incidence is in the *zOy* plane (conical diffraction).

tion of the theoretical values of the efficiencies in Fig. 11. The measured diffraction efficiency of the +1st order decreases from a value of 75% with an increasing conical angle of incidence. The calculated values were obtained by the modal method. The difference between theory and experiment can be explained primarily by the poor quality of the metallic coating.

5. Summary

We have presented a blazed reflection grating with a binary surface profile. The measured diffraction efficiency for TE polarization was 77%, whereas theory predicts an efficiency as great as 88% for the design used here. The grating can also be used as a polarizing beam splitter. It can separate TE- and TM-polarized light, because 77% of the TE-polarized light is deflected into the first diffraction order compared with 1% of the TE-polarized light that remains in the zeroth diffraction order. The diffraction efficiency for TM-polarized light under normal incidence was ~ 50%. The difference between theory and measurement appears because of an insufficiently thick metallic coating and can be reduced if better coating techniques are available.

The measurements with the CO_2 laser were performed at the Lehrstuhl für Fertigungstechnik (by M. Geiger), University of Erlangen, Germany. The authors are grateful for the help and for the permission to use equipment from the Laser Research Cooperative, Erlangen, Germany. One of the authors (J. T. Sheridan) is currently funded by the European Community. Part of the research was also funded by the Deutsche Forschungsgemeinschaft under Sondriforschungsbereich 182. Cooperation with Micronic Laser Systems AB, Sweden regarding the Laser Pattern Generator LPG-15P is gratefully acknowledged.

References

1. H. Haidner, P. Kipfer, W. Stork, and N. Streibl, "Höchstfrequente Gitter als Gradienten Index Elemente," presented at the Conference on the Deutsche Gesellschaft für Angewandte Optik, Oldenburg, Germany, 1991.
2. W. Stork, N. Streibl, H. Haidner, and P. Kipfer, "Artificial distributed index media realized by zero-order gratings," Opt. Lett. **16,** 1921–1923 (1991).
3. M. W. Farn, "Binary gratings with increased efficiency," Appl. Opt. **31,** 4453–4458 (1992).
4. W. E. Kock, "Metallic delay lenses," Bell Syst. Tech. J. **27,** 58 (1948).
5. A. F. Harvey, *Microwave Engineering* (Academic, London, 1963), Chap. 13.
6. G. F. Hull, "Microwave experiments and their optical analogues," in *Concepts of Classical Optics,* J. Strong, ed. (Freeman, San Francisco, Calif., 1958).
7. H. Haidner, J. T. Sheridan, J. Schwider, and N. Streibl, "Design of a blazed grating consisting of metallic subwavelength binary grooves," Opt. Commun. **98,** 5–10 (1993).
8. M. Neviere, P. Vincent, and R. Petit, "Sur la theorie du reseau conducteur et ses applications a l'optique," Nouv. Rev. Opt. **5,** 65–77 (1974).
9. T. Sandstrom and J. K. Tison, "Highly accurate pattern generation using acousto-optical deflection," in *Optical/Laser Microlithography IV,* V. Pol, ed., Proc. Soc. Photo-Opt. Instrum. Eng. **1463,** 629 (1991).
10. M. Heissmeier, U. Krackhardt, and N. Streibl, "Deep etching of microoptical components using self-aligned multiple masks," submitted to Appl. Opt.
11. G. Hass and L. Hadley, "Optical properties of metals," in *American Institute of Physics Handbook,* D. E. Gray, ed. (McGraw-Hill, New York, 1963), p. 112.
12. J. R. Andrewarta, J. R. Fox, and I. J. Wilson, "Resonance anomalies in the lamellar grating," Opt. Acta **26,** 69–89 (1979).
13. D. Maystre and R. Petit, "Diffraction par un reseau lamellaire infiniment conducteur," Opt. Commun. **5,** 90–93 (1972).
14. J. Miller, J. Turunen, M. Taghizadeh, A. Vasara, and E. Noponen, "Rigorous modal theory for perfectly conducting lamellar gratings," in *Holographics International '92,* Y. N. Denisyuk and F. Wyrowski, eds., (Institute of Electrical Engineers, Edinburgh, 1991), p. 99.
15. H. Kobolla, J. T. Sheridan, E. Gluch, J. Schwider, and N. Streibl, "Mixed polarization 2-D holographic permutation elements," Proc. Soc. Photo-Opt. Instrum. Eng. **1732,** 268–277 (1992).
16. R. Petit, ed., *Electromagnetic Theory of Gratings* (Springer-Verlag, Berlin, 1980), p. 31.
17. P. Kipfer, M. Collischon, H. Haidner, J. Sheridan, J. Schwider, N. Streibl, and J. Lindolf, "Infrared optical components based on a microrelief structure," Opt. Eng. **33,** 79–84 (1994).